Regulation of Stem Cell Function in an Engineered Vocal Fold-Mimetic Environment

Aidan B. Zerdoum,[1] Pooya Saberi,[2] Alexander J. Stuffer,[3] Dakota J. Kelly,[1] Randall L. Duncan,[3] Luc Mongeau,[2] Xinqiao Jia[1,3,4,5]*

[1]Department of Biomedical Engineering, University of Delaware, Newark, DE 19716, USA

[2]Department of Mechanical Engineering, McGill University, Montreal, Quebec, H3A 0C3, Canada

[3]Department of Biological Sciences, University of Delaware, Newark, DE 19716, USA

[4]Department of Materials Science and Engineering, University of Delaware, Newark, DE 19716, USA

[5]Delaware Biotechnology Institute, University of Delaware, Newark, DE 19711, USA

* Corresponding author and reprint requests

Xinqiao Jia, Ph.D., 201 DuPont Hall, University of Delaware, Newark, DE, 19716, Phone: 302-831-6553, Fax: 302-831-4545, E-mail: xjia@udel.edu

ABSTRACT. Human mesenchymal stem cells (hMSCs) have been proposed as therapeutic cells for the treatment of vocal fold (VF) scarring. Although functional recovery was observed in animal models after stem cell injection, it is not clear how injected stem cells interact locally with the extracellular matrix (ECM) of the lamina propria (LP) and how such interactions affect stem cell behaviors to improve function. Herein, we developed an *in vitro* cell culture platform where hMSCs were encapsulated in a LP-mimetic matrix, derived from hyaluronic acid (HA), poly(ethylene glycol) (PEG) and collagen, and cultured dynamically in a custom-designed VF bioreactor. The cell culture system was characterized by oscillatory shear rheology, laser doppler vibrometry (LDV), and digital image correlation (DIC). A constitutive finite element analysis (FEA) model was further developed to predict vibratory responses of the hydrogel. LDV analysis demonstrated an average displacement of 47 μm in the center of the hydrogel construct at 200 Hz applied frequency without any harmonics. The predicted strains throughout the hydrogel ranged from 0 to 0.03, in good agreement with reported values for the VF. The 3D cellular construct was subjected to vibrational stimulations at 200 Hz for an optimized duration of 1 h, as confirmed by a maximal c-Fos upregulation at the transcript level. Vibrational culture over a 3-day period with a 1h-on/1h-off pattern did not compromise the overall cell viability, but resulted in a significant downregulation of fibrogenic markers and diminished staining for alpha smooth muscle actin (αSMA). Collectively, high frequency mechanical loading resulted in the loss of myofibrogenic potential and a shift away from a fibrotic phenotype.

Keywords. Mesenchymal stem cells, vibration, bioreactor, vocal fold, fibrosis

Lay Abstract. This paper describes the construction and characterization of a cell culture system that recreates the condition and environment found in human vocal folds. The bench-top model system is advantageous because it overcomes difficulties associated with the usage of human subjects and excised human vocal fold tissues. This platform allows us to systematically investigate how stem cells introduced to the vocal fold respond to the chemical and mechanical environment of the tissue. We evaluated cell functions by analyzing gene expression and protein production. Our results show that, when maintained in a soft, tissue-mimicking matrix, and stimulated with mechanical signals generated during normal speech, stem cells do not adopt the behaviors of mature and specialized cells involved in wound contraction. Future works will focus on the identification of programs cells employ to respond to mechanical signals, as well as therapeutic drugs for the treatment of vocal fold scarring.

1. INTRODUCTION

The human vocal folds (VFs) are a pair of opposing tissues spanning the larynx. During phonation, the VFs open and close in a wave-like motion modulated by the airflow through the windpipe. The VF consists of a loose connective tissue, the lamina propria (LP), overlying the vocalis muscle and covered by a stratified squamous epithelium. Based on the relative content of fibrous proteins, such as elastin and collagen, the LP is divided into three layers – the superficial (SLP), intermediate (ILP), and deep lamina propria (DLP). In direct contact with the epithelium, the SLP is the softest, and has the lowest concentration of fibrous proteins [1]. In all layers of the LP collagen fibers are organized in an anisotropic fashion, parallel to the length of the VF. The SLP contributes to the propagation of the mucosal wave and shields the lower layers from microstructural damage due to the large impact forces generated during phonation [2, 3]. The ILP has the highest elastin content, whereas collagen is most abundant in the DLP. Variation in fibrous protein concentration reflects a change in tissue stiffness with depth, with the DLP mechanically matched to the underlying muscle layer. Hyaluronic acid (HA), a non-sulfated glycosaminoglycan, is enriched in the ILP. *Ex vivo* characterization of excised tissues shows that the LP exhibits a shear elastic modulus of 10 Pa – 3,500 Pa, depending on the depth of the LP [3-5].

Maintaining high tissue compliance is critical for proper sound production. Once phonation is initiated, the VFs sustain the oscillatory motion at a fundamental frequency (f_0). During normal human speech, the VFs experience an average f_0 of 100-300 Hz depending largely on age and gender [6]. The highly specialized tissue structure of the LP infers that changes to VF pliability can result in dysphonia, or loss of normal phonatory capability. The initiation of the wound healing process in VFs results in the release of cytokines that promote the infiltration of the wound site by cells of mesenchymal origin.[7, 2] After exposure to pro-fibrotic signals, such as transforming

growth factor β1 (TGFβ1) and connective tissue growth factor (CTGF), these cells deposit fibrous proteins, adopt a myofibroblastic phenotype, and facilitate wound contraction. A prolonged wound healing response in VF tissue, as a result of corrective surgery, trauma, overuse, or misuse, can lead to fibrosis – buildup of fibrotic tissue that results in scar formation. Scarred VF exhibits a higher elastic modulus than healthy tissue, causing an increase in the minimum pressure needed to drive VFs into oscillation [8].

Preclinical animal studies have shown favorable treatment outcomes for vocal fold scarring using mesenchymal stem cells (MSC) harvested from bone marrow or adipose tissue [9-12]. Outcome measures generally include the gross tissue structure, the viscoelastic parameters and the phonatory functions of the tissue. Because the VFs are housed deep within the larynx and are vulnerable to surgical manipulations, mechanistic investigations on the fate of injected MSCs are challenging. Moreover, healing responses observed in animal models differ from human pathophysiology [13]. Therefore, there is a need for a physiologically relevant *in vitro* cell culture platform that allows straightforward interrogation of molecular and cellular mechanism contributing to the understanding of MSC-based regenerative therapy for the treatment of vocal fold scarring.

We have previously developed a vocal fold bioreactor capable of generating vibratory stimulations at human phonation frequencies [14, 15]. Vibration was generated electromagnetically and translated to the cell culture chamber by oscillatory air pressure. In our early studies, human MSCs (hMSCs) were cultured on fibronectin-coated, electrospun poly(ε-caprolactone) (PCL) mats and were subjected to vibratory stimulations at 200 Hz with a 1h-on 1h-off pattern for a total of 7 days. The vibratory stimulation significantly up-regulated genes encoding VF-relevant ECM proteins, but down-regulated alternative hMSC differentiation marker

expression. In these studies, hMSCs were cultured on 2D in direct contact with synthetic fibers that are several orders of a magnitude stiffer than the LP. Thus, cellular responses may not be physiologically relevant.

Herein, hMSCs were cultured in 3D in semi-synthetic hydrogel that more closely recapitulates the composition and mechanical properties of the native ECM of the LP. The hydrogel is composed of a covalent HA/poly(ethylene glycol) (PEG) network entrapping assembled collagen fibrils. Based on the composition, these materials are referred to as HPC gels. Our previous work showed that hMSCs cultured statically in HPC gels were phenotypically reminiscent of cells involved in the wound healing process [16]. To understand the effects of phonation on hMSC differentiation, cell-laden HPC gels containing 2 mg/ml collagen (HPC2 gels) were cultured in the vibrational bioreactor. Experimental and computational methods were applied to characterize hydrogel displacement within the bioreactor. Our results show that high-frequency mechanical stimulation suppressed the development of a myofibroblastic phenotype from hMSCs.

2. MATERIALS AND METHODS

2.1. Hydrogel Synthesis. The HPC gels were created as previously described [16]. Briefly, thiolated HA (HA-SH, 20 mg/ml), collagen type I (4 mg/ml) at pH 8.2, and polyethylene glycol diacrylate (PEG-DA, 8 mg/ml) were combined at a volumetric ratio of 1:2:1. All gel components were kept ice-cold before mixing to ensure no collagen fibrillization occurred until the gelation process began. For cell encapsulation, hMSCs were pelleted and resuspended in the HA-SH component before addition of collagen and PEG-DA.

2.2. Bioreactor Assembly. The vibrational bioreactor was fabricated according to previously published specifications [17, 14]. The device was comprised of two aluminum bars, each holding four 3-inch extended range mini-woofers wired in pairs, all within an anti-humidity enclosure. Two polycarbonate blocks containing a sandwiched poly(dimethyl siloxane) (PDMS) disk were mounted above each mini-woofer. A 24-mm wide hole was drilled through each polycarbonate block to allow for transmission of air pressure oscillations from the speaker surface to the PDMS disk, and to permit facile media refreshment during dynamic cell culture. The PDMS disk with an entrenched circular envelope in the center (diameter: 12 mm) was prepared using Dragon Skin 20® platinum cure silicone rubber (Smooth-On Inc., Macungie, PA). The envelope held a 100-μL hydrogel directly above the speaker, preventing gel delamination from the PDMS membrane during vibrational culture, and allowing for greater transmission of vibratory stimulation through the thinner underlying layer. The paired polycarbonate blocks, the PDMS disk and the individual speaker combined are referred to as a vibration subassembly (Figure 1A). To eliminate external disturbance and to ensure consistency, PDMS disks were secured using a torque wrench to evenly tighten all screws on the polycarbonate blocks. External application of vibration during culture was minimized by surrounding polycarbonate blocks with silicone isolators. In order to maintain an aseptic environment while allowing for CO_2 and O_2 gas exchange, the vibration modules were covered with breathable AeraSeal film (MilliporeSigma, St. Louis, MO).

2.3. Laser Doppler Vibrometry (LDV). For surface measurements, an aluminum reflector (2 mm × 2 mm square) was secured to the center of the PDMS membrane using a double-sided tape. After the vibration chamber was filled with phosphate buffered saline (PBS, 1.5 ml), sinusoidal signal with a peak-to-peak voltage (V_{pp}) of 1 was introduced to the mini-woofer via a waveform

generator, and the membrane was driven into oscillation at 200 Hz. A Polytec (Irvine, CA) 100-V LDV unit was positioned at a 50 cm above the vibration subassembly, and the laser was focused on the reflector target. The oscillatory amplitude as a function of frequency was analyzed using VibSoft data acquisition software (Polytec). Resultant amplitude values were divided by a factor of 1.33 to account for the refractive index of PBS [18]. For in-gel measurements, 100 μL of the HPC gel solution was pipetted into the circular envelope within the PDMS disk, and the square aluminum reflector was suspended in the gelling liquid approximately 200 μm from the bottom. In-gel LDV studies included a control gel without collagen (HPC0). Thirty minutes after the gel components were mixed, PBS (1.5 mL) was added to the vibration chamber to mimic cell culture conditions. The LDV laser beam was focused onto the reflector surface and its oscillatory amplitude at 200 Hz was determined.

2.4. Digital Image Correlation (DIC). To perform DIC analysis, a randomized speckle pattern was created on the PDMS membrane by adding white silicone pigment (Silc Pig, Smooth-On) and black polyester particles (American Crafts) to the PDMS mixture during the membrane molding process. To ensure accurate DIC processing, images of the membranes taken while secured inside the vibrational subassembly were analyzed for gray value in Fiji image processing software to confirm normal distribution. High framerate video (4 k fps, 1280×1024 resolution) of the membranes under 200 Hz vibration was obtained using a high-speed camera (IDT MotionPro® Y4S) in order to resolve membrane movement at high frequencies. Resultant image sets were processed via VIC2D DIC software (Correlated Solutions) using a reference image of the membrane at rest for calibration. A polygonal region of interest (ROI) was defined to include the membrane envelope, and analysis was performed using a subset size of 50 pixels^2 and a step size

of 7 pixels. Strain was determined via correlation between the reference image and subsequent deformed images.

2.5. Computational Modeling. A computational model was used to estimate the time-dependent deformation and stresses within the vibration subassembly blocks. All simulations were performed using a commercial ANSYS software (ANSYS Mechanical, Ansys Inc., Canonsburg, PA). The model was based upon the geometry, material, and mechanical properties of the vibration subassembly. Two polycarbonate blocks were used to support a circular PDMS membrane (diameter: 42 mm, height: 1.2 mm). The hydrogel component was situated within the membrane envelope (diameter: 12 mm, height: 1 mm). External oscillatory amplitude of the vibrational subassembly was measured experimentally by LDV. This amplitude of vibration (Table S1) was applied to the polycarbonate blocks, which drove the hydrogel into oscillation similar to that observed under experimental conditions.

2.6. Cell Maintenance. Bone marrow-derived hMSCs (Lonza, Walkersville, MD) were purchased at passage 2 and expanded for use at passage 4. Cells were cultured and passaged according to manufacturer's protocol. Cell suspensions containing 1 million cells/ml were frozen in cryovials in LN_2 for further use. Cryovials were then thawed and hMSCs were seeded onto 182 cm^2 tissue culture-treated plastic at 5,000 cells/cm^2. Maintenance media (MSCGM, Lonza) was added and hMSCs were propagated at 37 °C, 5% CO_2, and 85% humidity for 7 days or until ~90% confluence, with media changes every 3 days.

2.7. 3D Vibratory Culture. Upon reaching confluence, hMSCs were lifted by adding 3 ml accutase cell dissociation reagent (Thermo Fisher Scientific, Waltham, MA) and transferring the resulting cell suspension to centrifuge tubes to be pelleted at 450 g for 5 minutes. These cell pellets were resuspended into a pH-adjusted HA-SH solution and collagen/PEG-DA were added to initiate gelation. Once encapsulated, maintenance media was changed on cell/gel constructs every 2 days. After hMSC encapsulation in HPC2 hydrogels, 1.5 ml maintenance media was added, and gels were precultured for 7 days. Following this preculture period, vibrational stimulation at 200 Hz and 1 V_{pp} speaker voltage for 5, 15, 30, 60, and 120 minutes was initiated. Immediately following the vibratory culture, constructs were immersed in ice-cold PBS then removed from the PDMS membranes and processed for RNA isolation and subsequent qPCR analysis. Long-term vibratory cell culture was executed similarly, vibrating constructs on a 1h-on/1h-off cycle for a total of 12 h per day for 3 days before collection for downstream processing. Static samples were cultured in identical vibration subassemblies to avoid differences in temperature and gas exchange.

2.8. Cell Viability. A commercially available cell viability staining kit was used to assay cell viability according to manufacturer's protocol (LIVE/DEAD, Thermo Fisher Scientific). A mixture containing 4 μM of both calcein AM and ethidium homodimer was prepared in PBS (1 ×). Cell/gel constructs were washed once with PBS, 1 ml of the LIVE/DEAD solution was added, and cells were incubated at 37 °C for 15 minutes. Finally, the dye solution was aspirated, hydrogels were washed twice with PBS, and images were taken of cell/gel constructs maintained under static and vibratory conditions using a confocal laser scanning microscope (Zeiss CLSM 710).Viable and dead cells were labeled and counted manually using the Cell Counter plugin in the Fiji image processing program.

2.9. Quantitative Real-Time Polymerase Chain Reaction (qPCR). Gene expression experiments were carried out using qPCR as described previously [16]. Cell/gel constructs were collected immediately following vibration and frozen in a dry ice/isopropanol slurry for storage at -80 °C until further use. To isolate RNA, pestles were used to pulverize the frozen samples into a fine powder, then 1 mL TriZol reagent and 200 µL chloroform were added. Samples were centrifuged at 15,000 g then the aqueous layer was aspirated and added to 500 µl of isopropanol before centrifugation at 12,000 g to pellet RNA. Pellets were washed in triplicate with 70% ethanol before resuspension in DEPC H_2O to determine RNA concentration and purity via spectrophotometry (Nanodrop-2000). Template cDNA was reverse-transcribed by the QuantiTect kit (Qiagen) according to manufacturer's protocol. Amplification of template cDNA (4 ng) with specific primers (400 nM) for each gene target in the presence of Power SYBR Green master mix (Invitrogen, Carlsbad, CA) was performed in an ABI 7300 real-time sequence detection system. Detailed information on primers used in qPCR analysis, along with abbreviations for tested genes, is summarized in Table 1. Glyceraldehyde-3-phosphate dehydrogenase (GAPDH) was utilized as a reference target. Resulting qPCR data were normalized and processed using commercially available qbase+ software.

2.10. Immunohistochemistry. Following vibrational stimulation, hydrogels were immediately rinsed with ice-cold PBS, then incubated in 4% PFA solution for 20 minutes. Once fixed, cell/gel constructs were washed twice with PBS containing 0.05% Tween-20 (PBST) then blocked in 3% bovine serum albumin (BSA) in PBS overnight at 4°C. After the blocking step, FITC-conjugated monoclonal α-smooth muscle actin (αSMA, Sigma) antibody (diluted 1:100) and

Alexa Fluor 568-conjugated phalloidin (Thermo Fisher, diluted 1:400) in 3% BSA were added and allowed to incubate for 2 h at room temperature. Next, samples were washed in triplicate with PBST, and DAPI (Millipore, 1:500 dilution) was added for 10 minutes at room temperature. Samples were stored in PBS for imaging via confocal laser scanning microscopy (Zeiss LSM 880 with Airyscan).

2.11. Statistical Analysis. All quantitative analyses were conducted on data sets in which n =3 or 4. A student's T-test or one-way analysis of variance (ANOVA) with Tukey-Kramer post-hoc analysis ($p < 0.05$ considered significant) was utilized to test for significance unless where indicated. Results are presented as mean ± standard error. When multiple groups were compared, groups labeled with different letters indicate significance.

3. RESULTS

3.1. Bioreactor Characterization.

The vocal fold bioreactor (Figure 1A) was composed of two metal bars, each housing four parallel vibration subassemblies. The individual subassembly was directly mounted on top of a speaker controlled by a speaker selector. A watertight vibration chamber was created by sandwiching a PDMS disk between a pair of hollow polycarbonate blocks. The vibrational signals were translated to the chamber by the oscillating air pressure underneath. The vibration units and speaker selector were enclosed in an anti-humidity chamber. The assembly, containing 1-4 (Figure 1A), was housed in the cell culture incubator, while the power amplifier and the function generator were placed outside [14, 15, 17].

LDV measures the magnitude of a Doppler frequency shift of a light source caused by a dynamically oscillating surface. First, measurements at the center of the PDMS membrane were taken while increasing the peak-to-peak voltage (V_{pp}) supplied to the speaker. The amplitude of displacement at discrete frequencies was determined by performing a fast Fourier transform (FFT) on the output signal across a bandwidth from 0-500 Hz at 1.2 kHz sampling frequency. The average mid-membrane displacement amplitude (distance traveled during oscillation) at 200 Hz was 56 ± 2 μm at 0.5 V_{pp}, reaching a maximum of 74 ± 2 μm at 1 V_{pp} (Figure 1B). Above 1 V_{pp}, PBS within the vibration subassembly became turbulent and was ejected from the cell culture well. Thus, speaker voltage was maintained at 1 V_{pp} for cell culture studies. Analysis of the full frequency range of LDV measurements showed a peak amplitude of 74 μm at 200 Hz, and below 5 μm at all other frequencies (Figure 1C). This result demonstrates that there is minimal resonance occurring at harmonic frequencies (100 Hz, 400 Hz). To measure the in-gel oscillation, reflector targets were embedded within the HPC2 gel construct. This resulted in a reduction of the measured amplitude to 47 ± 3.6 μm. Removing the collagen component from the HPC gels led to a significantly lower measured amplitude (61 ± 0.6 μm, Figure 1D), confirming the damping effect of the added collagen fibrils.

DIC coupled with high-speed imaging allowed for characterization of equivalent strain across PDMS membranes when driven into oscillation at high frequencies. The equivalent strain is the net magnitude of strain at each point within the area of interest. DIC uses correlations between grayscale patterned images to determine deformation over time. The majority (84%) of strains over the surface of the membrane were lower than 0.01, with maximum strains of 0.03 occurring around the central envelope periphery (Figure 2A). The distribution of resultant equivalent strains across the central envelope of the PDMS membrane was plotted (Figure 2B). Strain distribution had a

rightward skew, meaning values were biased towards lower strains (<0.005). The average strain was 0.0051, with a standard error of ± 5.8×10^{-5}.

The bioreactor was further characterized by Finite Element Analysis (FEA). Maximum displacement amplitudes of the surface of the upper polycarbonate block at various frequencies were recorded during LDV analyses when the subassembly was driven into vibration at 200 Hz. These data were then applied as boundary conditions at the outer surfaces of the frames. The input displacement amplitudes are reported in Table S1. The predicted equivalent strains directly on the PDMS surface were then plotted in a histogram for comparison with DIC data (Figure 2C). Dimensions for vibration subassembly components were measured and applied to the model geometry (Figure 3A). The blocks, silicone membrane, and the gel matrix were set to be bonded at their contact surfaces. The domain geometry consisted of 102,200 second-order hexahedral elements (197,064 nodes). These elements allowed for high resolution of material deformations and strains. To reproduce the boundary conditions of the vibration subassembly, the stiffness of the blocks was matched to that for polycarbonate. Isotropic material properties were determined for the PDMS membrane via rheometric analysis. These material properties are summarized in Table S2.

A third order Ogden hyperelastic model was used to describe the stress-strain response of the hydrogel. A fit to the rheometric shear strain sweep tests was performed to find material parameters (α_p and μ_p, Table S3). using the ANSYS curve fitting tool (Engineering Data, Ansys Inc., Canonsburg, PA). The resultant material parameters were used in the strain energy density calculation (Equation 1)[19];

$$\psi = \sum_{n=1}^{N} \left(\frac{\mu_p}{\alpha_p}\right) [\lambda_1^{\alpha_p} + \lambda_2^{\alpha_p} + \lambda_3^{\alpha_p} - 3], \qquad \text{Equation 1}$$

where ψ is the strain energy density and λ_i are the principal stretches.

Rayleigh damping was included in the model to account for energy dissipation within the PDMS and hydrogel components under dynamic loading (Table S4). A fit to frequency sweep data from rheometric measurements was used to calculate α and β parameters. The α and β parameters were used as correction factors in mass and stiffness matrices respectively (Equation 2)[20];

$$[C] = \alpha[M] + \beta[K], \qquad \text{Equation 2}$$

where [C] is the damping matrix, [M] the mass matrix and [K] is the stiffness matrix. The effective damping ratio, ξ_i, for a natural circular frequency of mode I, ω_i, can be calculated by (Equation 3)[20];

$$\xi_i = \alpha/2\omega_i + \beta\omega_i/2. \qquad \text{Equation 3}$$

The finite element model was solved using a 0.1 ms time step for 0.2 seconds. Verification studies were then performed to ensure the accuracy of the results with respect to mesh size and time steps. The predicted values of in-gel amplitude in the center of the membrane at a height of 0.5 mm into the gel were matched to their corresponding experimental values, as determined by LDV (Figure 3B-C). Both the simulation and experimentally generated displacements were highest at 200 Hz, with negligible amplitudes at harmonic frequencies. The mean in-gel amplitude measured by LDV was 47.0 ± 3.6 μm compared to a predicted value of 31 μm. The slight decrease in predicted amplitude is likely due to the usage of rheological data obtained at 0.1-10 Hz used to

fit the Rayleigh damping parameters. The FEA model was then used to predict strain within the hydrogel component. Equivalent strains ranged from 0-0.03 within the hydrogel, with higher strain found in the center of the gel and around the periphery (Figure 3D, Movie S1, S2). The FEA results confirmed the overall trend seen experimentally by LDV and DIC.

3.2. Vibratory Culture.

hMSCs were encapsulated in HPC2 gels and were maintained statically for 7 days in the bioreactor before the vibratory stimulation was introduced. Constructs were vibrated for 3 days at a frequency of 200 Hz, with a 1h-on/1h-off pattern for a total of 12 h per day. hMSCs maintained a high viability and adopted a spindle shaped morphology when the experiment was terminated at day 10 (Figure 4A-B). To confirm there was no significant difference in cell viability, cells LIVE/DEAD cell viability dye in representative images from vibrated and static samples were counted using the Cell Counter plugin in the Fiji biological image processing software. As a control, static samples from day 7 (before vibration) were also counted. Our results show that 77.0 ± 5.7% of cells were viable by the end of the 7-day preculture. After three days of vibration, 78.0 ± 2.4% and 81.0 ± 2.1% of cells were viable in static and vibrated samples, respectively (Figure 4C). Based upon the quantified viability percentages, there was no statistically significant difference in cell viability due to the 3-day vibratory stimulation.

A time course study was undertaken to determine the optimal application of vibrational stimulations to promote cellular mechanotransduction (Figure 5A). c-Fos was chosen as the marker gene for activation due to its immediate and transient response [21-24]. c-Fos expression remained relatively constant for the first 15 min of vibration, increasing only slightly to 1.25 ± 0.27-fold and 1.12 ± 0.09-fold over static controls for 5- and 15-min treatments, respectively. At 30 min,

expression increased significantly to 2.82 ± 0.38-fold. After 60 min of vibration, the highest significant upregulation was observed, reaching 6.30 ± 0.9-fold compared to static controls ($p<0.05$). Extending the vibration to 120 min resulted in a moderate decrease in c-Fos expression, but compared static controls, the expression remained high (3.13 ± 0.52-fold, Figure 5B). c-Fos upregulation coincided with a downregulation of CTGF at 30 and 60 min (0.24 ± 0.10 and 0.29 ± 0.07-fold respectively, Figure 5C), however expression for MMP1 and MMP2 were not significantly affected. At 120 min, there was a concurrent upregulation of other immediate early genes EGR1 (1.71 ± 0.16-fold) and c-Jun (0.65 ± 0.10-fold), but the 60-min treatment resulted in significantly more upregulation of EGR1 at 2.26 ± 0.16-fold compared to static control (Figure 5D, $p<0.05$).

Next, qPCR studies were performed to study the transcriptional response of hMSCs to vibratory stimulation at a longer timescale. Cell/gel constructs were vibrated at 200 Hz on a 1-h on/1-h off pattern for 12 h per day for three days. Based on an in-gel amplitude of 47 μm, this constitutes a total distance traveled of 609 m by hMSCs over the three-day dynamic culture. On day 10 following vibration, the expression of p53 (Figure 6B), a regulator of cell apoptosis, was unchanged relative to static controls at the same time point (0.78 ± 0.14-fold vs 1.01 ± 0.16-fold, respectively). Dynamic oscillation resulted in significant downregulation of genes commonly associated with fibrogenesis. A significant downregulation ($p<0.05$) was observed for fibronectin (FN, 0.68 ± 0.10-fold), collagen type I α1 (COL1α1, 0.26 ± 0.11-fold), collagen type III α1 (COL3α1, 0.26 ± 0.30-fold), α-smooth muscle actin (αSMA, 0.10 ± 0.68-fold), and lysyl oxidase (LOX, 0.51 ± 0.35-fold). In addition, vascular cell adhesion molecule was downregulated (VCAM, 0.13 ± 0.04-fold) compared to static controls. Meanwhile, a significant upregulation was observed in mRNA targets encoding early growth response 1 (EGR1, 4.42 ± 0.40-fold), c-Fos (2.39 ± 0.19-

fold), hyaluronic acid synthase 1 (HAS1, 2.52 ± 0.22-fold), melanoma cell adhesion molecule (MCAM, 2.11 ± 0.19-fold), and cyclooxygenase 2 (COX2, 67.9 ± 0.71-fold). Gene targets which showed no significant change were the EDA-domain of FN (FNEDA, 0.76 ± 0.04-fold), matrix metalloproteinases (MMP1 and MMP2, 1.61 ± 0.28 and 0.96 ± 0.10-fold, respectively), transforming growth factor β1, (TGFβ1, 1.37 ± 0.31-fold), integrin β1 subunit (ITGβ1, 0.94 ± 0.08-fold), and connective tissue growth factor (CTGF, 0.57 ± 0.10-fold).

Immunofluorescence was utilized to confirm αSMA downregulation. Under static conditions, αSMA was incorporated into F-actin stress fibers running parallel along the cell body (Figure 7, white arrowheads), indicative of myofibroblastic phenotype.[7, 25] Comparison of immunofluorescence images for vibrated samples against the static controls revealed that, following vibration, the expression of αSMA and the development of F-actin stress fibers was significantly diminished. Thus, vibrational signals suppressed hMSCs commitment to myofibroblasts.

4. DISCUSSION

Due to their histocompatibility, self-renewal, and regenerative capabilities, hMSCs has been suggested as therapeutic cells for the treatment of VF scarring. Previous animal studies showed that injection of MSCs to scarred VF resulted in reduced production of collagen type I and recovery of tissue functionality, despite an overall low survival rate for injected cells [9-11]. Using an HA/PEG/collagen composite hydrogel and a vibrational bioreactor, this work aims to understand how the unique biochemical and biomechanical environment of the VF affects the phenotype and function of injected hMSCs. Prior to 3D dynamic culture, the bioreactor was characterized collectively by LDV, DIC and FEA. LDV analysis showed that all eight vibration subassemblies

exhibited a consistent mid-membrane displacement amplitude of 74 ± 2 μm at 200 Hz and 1 V_{pp}, with no harmonics present. Thus, the desired input frequency from the waveform generator was isolated, and the observed cellular responses were frequency specific. Further dynamic analysis by DIC showed a distribution of strains across the membrane surface from 0 to 0.03. Within the bulk of the HPC2 gel, the measured amplitude decreased due to the ability of entrapped collagen fibrils to dissipate energy.

A FEA model was developed to estimate strain distribution throughout the hydrogel network under dynamic oscillation. Rheological data of the cell-free HPC gels were utilized for curve-fitting analysis as previous studies have shown that the encapsulated cells do not contribute significantly to bulk viscoelastic properties [26-29]. The predicted strains varied from 0-0.03 within the gel, and the distribution of strains predicted along the surface of the PDMS membrane followed similar trends compared to DIC measurements (Figure 2C). Areas of high strain were found 1.5 and 6 mm from the gel edge and 0.5 mm above the PDMS membrane. Using uniaxial tensile testing and a constitutive model, researchers determined that the strain experienced within the VF SLP ranges from 0-0.0443 [30], in good agreement with the predicted vibrational strains introduced in our bioreactor. Separately, LDV analysis showed that, relative to the static state with no airflow, the vocal fold surface oscillates from 64 to 188 μm during phonation. Of note, the epithelial layer typically undergoes larger deformations than the underlying SLP [31]. Our in-gel LDV measurement showed a slightly lower displacement of 47 ± 4 μm.

Maintaining high cell viability is a prerequisite for developing a physiologically relevant tissue model. hMSCs cultured in the bioreactor remained highly viable throughout the duration of culture and the percent viable cells was not affected by vibrational stimulation. The insensitivity of the expression of p53, a regulator of cell apoptosis, to vibration further confirmed the

cytocompatibility of the bioreactor. These observations are in good agreement with results from our previous studies where hMSCs were cultured on fibrous PCL scaffolds and subjected to a similar vibration stimulation [15, 17]. Webb and coworkers studied the effects of vibrational stimulation on 3D encapsulated fibroblasts and found that vibration significantly decreased cell viability over time [32]. In this study, fibroblasts were maintained in a HA hydrogel containing immobilized RGD and vibration was generated mechanically, rather than acoustically, using a voice coil actuator [33]. The higher oscillatory strain introduced to the cell/gel constructs may have compromised the overall cell viability [34].

The mitogen-activated protein kinase (MAPK) pathway is involved when an external mechanical signal is transmitted to the cell nucleus to elicit transcriptional changes. This pathway is initiated by engagement and subsequent mechanical stimulation of integrin receptors, and results in the phosphorylation of several downstream effectors, including extracellular signal-regulated kinase 1/2 (ERK1/2). Activation of this kinase leads to induction of the AP-1 complex, specifically through proto-oncogene c-Fos [23]. In this study, a 7-day preculture period was chosen to allow for the establishment of integrin-mediated matrix engagement [16]. c-Fos was chosen as an immediate-early gene because it is typically upregulated rapidly in response to a wide variety of external stimuli [23]. One-hour vibration at 200 Hz was sufficient to cause a significant upregulation of the c-Fos gene. The expression of a co-transcriptional factor, c-Jun, and an additional regulator of ERK1/2 mechanotransduction, EGR-1, were similarly upregulated compared to static controls, providing additional evidence for cell activation at the 1-h time point. By 2 h, immediate-early genes were still upregulated, although at a lower expression level. These results indicate that early cell transcriptional response to vibration at 200 Hz was triggered after a 30-min treatment and further treatment beyond 1 h led to a decline in cell response. Thus, for

subsequent long-term culture studies, cells were stimulated with a 1h-on/1h-off cycle to ensure activation of mechanotransduction signaling cascades.

Following 3-day vibrational culture, hMSCs encapsulated in HPC2 hydrogels decreased expression of fibrous proteins COL1α1 and COL3α1, as well as αSMA. Downregulation of αSMA was further confirmed by immunofluorescence. A decrease in expression of these three markers of myofibroblastic differentiation indicates that hMSCs shifted away from a profibrotic, myofibroblastic phenotype. In addition, the expression of HAS1 increased with vibration. HAS1 has been shown to promote dermal tissue regeneration by lowering the inflammatory response and inducing production of a more organized collagen fibrillar structure [35, 36]. Decreased fibrogenesis coupled with increases in HA expression can be indicators of scarless wound healing [37, 38]. This observation is supported by studies involving application of vibratory stimulation by shockwave therapy and ultrasound that can augment healing effects of native cell types [39-41]. In a similar speaker-driven vibratory study conducted on 2D vocal fold fibroblast cultures, Kirsch *et al.* found an increase in fibrogenesis and HAS1 expression but no change in αSMA [42]. Interestingly, cells in 2D culture on stiff PDMS upregulated collagen I and III expression following vibration while our 3D soft hydrogel culture system caused downregulation, highlighting the necessity for a dimensionally and mechanically relevant model of VF connective tissue to more accurately predict physiological response. VCAM and MCAM, two cell adhesion molecules, exhibited conflicting changes in expression under mechanical loading. The upregulation of MCAM is associated with hMSC stemness and indicates that cells are moving back towards a more progenitor-like state [43, 44]. VCAM is a well-known regulator of hMSC motility through its interactions with integrins as well as the actin cytoskeleton [45, 46].

Transcriptional analysis of the inflammatory marker COX2 revealed significant upregulation following the 3-day vibratory period. COX2 typically becomes upregulated in response to cellular strain and other stressors [47]. Petkova *et al.* performed a study on COX2 signaling in lung fibrosis and found that a lack of functional COX2 expression resulted in increased proliferation and collagen production through decreased prostaglandin E_2 (PGE2) activation [48]. A similar study agreed with these results in a mouse model of intestinal fibrosis following treatment with the COX2 inhibitor celecoxib [49]. Branksi *et al*. studied cyclic tensile strain (CTS, 0.5 Hz, up to 18% strain) and observed downregulated COX2 expression in VFFs in addition to increased COL1 expression, which would indicate fibrogenesis [50]. Overall, this study presents a mechanical method of inhibiting the fibrotic response of hMSCs in a 3D hydrogel culture without affecting cell viability.

Under our 3D culture conditions, vibratory stimulations did not result in significant changes in the expression of MMP1 and 2 at the mRNA level. It is possible that hMSCs cultured in HPC2 gels were not as catabolically active as tissue-resident stem cells involved in tissue repair during wound healing [51]. Alternatively, MMP expression may be transient and time-dependent and our short-term (5 min to 120 min) and 3-day (1 h on/1 h off) vibration regimen may not capture the moment when MMP expression is significantly upregulated. Finally, post-transcriptional regulatory processes [52] may lead to changes in MMPs that cannot be detected by qPCR.

In this study, we investigated how vibratory stimulations affect phenotype of hMSCs cultured in a soft HPC2 matrix. Our previous work on dynamic culture of hMSCs on a stiff, fibrous PCL scaffold showed a different gene expression pattern in response to similar vibration conditions.[15] Thus, matrix stiffness may dictate cellular response to vibration. The bioreactor described here is not intended to completely replicate the complex biomechanical environment of the native tissue.

The engineered, VF-mimetic environment enabled us to identify how a specific, physiologically relevant and individually controlled mechanical perturbation affects the phenotype and function of hMSCs. We are currently developing a hydrogel-based cellular model of scarred vocal folds and evaluating how hMSCs respond to a more complex mechanical stimulation that combines low frequency, high strain tensile stretch with high frequency, low strain oscillation.

CONCLUSION:

hMSCs were cultured in an engineered, VF-mimetic matrix in the presence of vibratory stimulations at human phonatory frequencies. The mechanical signals generated in the bioreactor was measured by LDV and DIC, and a constitutive FEA model was developed to predict strains generated in the hydrogel matrix. A 1-h vibration at 200 Hz resulted in the upregulation of an immediate-early response gene, c-Fos. Application of a 1-h on/1-h off cycle to the cell-laden construct over a 3-day period resulted in the down regulation of genes encoding FN, Col1α1, Col3α1, LOX, αSMA, and VCAM, but an upregulation of genes encoding EGR1, c-Fox, HAS1, MCAM and COX2. Immunofluorescent analysis revealed a decrease in αSMA following the 3-day vibratory culture. Our results indicate that vibrational stimulations resulted in a decrease in myofibroblast transition while increasing scar turnover. Overall, this study confirms a specific mechanical regimen capable of reversing fibrogenic phenotype to direct potential therapeutic treatments following VF scarring.

ACKNOWLEDGMENT

This work was funded in part by National Institutes of Health (NIH, R01 DC014461), the National Science Foundation (NSF, DMR 1809612) and the Delaware Bioscience Center for

Advanced Technology (CAT). We acknowledge the Delaware COBRE program (NIH, P30 GM110758), the Delaware INBRE program (NIH, P20 GM103446) and the Bioimaging Center at Delaware Biotechnology Institute (NIH, S10 OD016361) for instrumentation support. ABZ acknowledges funding support from the NSF Integrative Graduate & Research Traineeship (IGERT) Program.

References:

1. Gray SD. Cellular physiology of the vocal folds. Otolaryngol Clin North Am. 2000;33(4):679-98. doi:10.1016/S0030-6665(05)70237-1.
2. Branski RC, Verdolini K, Sandulache V, Rosen CA, Hebda PA. Vocal fold wound healing: a review for clinicians. J Voice. 2006;20(3):432-42. doi:10.1016/j.jvoice.2005.08.005.
3. Chan RW, Gray SD, Titze IR. The importance of hyaluronic acid in vocal fold biomechanics. Otolaryngol Head Neck Surg. 2001;124(6):607-14. doi:10.1177/019459980112400602.
4. Goodyer E, Hemmerich S, Muller F, Kobler JB, Hess M. The shear modulus of the human vocal fold, preliminary results from 20 larynxes. Eur Arch Otorhinolaryngol. 2007;264(1):45-50. doi:10.1007/s00405-006-0133-8.
5. Jiao T, Farran A, Jia X, Clifton RJ. High Frequency Measurements of Viscoelastic Properties of Hydrogels for Vocal Fold Regeneration. Exp Mech. 2009;49(2):235-46. doi:10.1007/s11340-008-9126-4.
6. Fouquet M, Pisanski K, Mathevon N, Reby D. Seven and up: individual differences in male voice fundamental frequency emerge before puberty and remain stable throughout adulthood. Royal Society Open Science. 2016;3(10).
7. Branco A, Bartley SM, King SN, Jette ME, Thibeault SL. Vocal fold myofibroblast profile of scarring. Laryngoscope. 2016;126(3):E110-7. doi:10.1002/lary.25581.
8. Jette ME, Hayer SD, Thibeault SL. Characterization of human vocal fold fibroblasts derived from chronic scar. Laryngoscope. 2013;123(3):738-45. doi:10.1002/lary.23681.
9. Svensson B, Nagubothu RS, Cedervall J, Le Blanc K, Ahrlund-Richter L, Tolf A et al. Injection of human mesenchymal stem cells improves healing of scarred vocal folds: analysis using a xenograft model. Laryngoscope. 2010;120(7):1370-5. doi:10.1002/lary.20926.
10. Svensson B, Nagubothu SR, Cedervall J, Chan RW, Le Blanc K, Kimura M et al. Injection of human mesenchymal stem cells improves healing of vocal folds after scar excision--a xenograft analysis. Laryngoscope. 2011;121(10):2185-90. doi:10.1002/lary.22143.
11. Hertegard S, Cedervall J, Svensson B, Forsberg K, Maurer FH, Vidovska D et al. Viscoelastic and histologic properties in scarred rabbit vocal folds after mesenchymal stem cell injection. Laryngoscope. 2006;116(7):1248-54. doi:10.1097/01.mlg.0000224548.68499.35.
12. Ohno S, Hirano S, Kanemaru S, Mizuta M, Ishikawa S, Tateya I et al. Role of circulating MSCs in vocal fold wound healing. Laryngoscope. 2012;122(11):2503-10. doi:10.1002/lary.23543.

13. Bless DM, Welham NV. Characterization of vocal fold scar formation, prophylaxis, and treatment using animal models. Curr Opin Otolaryngol Head Neck Surg. 2010;18(6):481-6. doi:10.1097/MOO.0b013e3283407d87.
14. Zerdoum AB, Tong Z, Bachman B, Jia X. Construction and characterization of a novel vocal fold bioreactor. J Vis Exp. 2014(90):e51594. doi:10.3791/51594.
15. Tong Z, Zerdoum AB, Duncan RL, Jia X. Dynamic vibration cooperates with connective tissue growth factor to modulate stem cell behaviors. Tissue engineering Part A. 2014;20(13-14):1922-34. doi:10.1089/ten.TEA.2013.0496.
16. Zerdoum AB, Stuffer AJ, Heris HK, Liu S, Mongeau L, Duncan RL et al. Culture of Mesenchymal Stem Cells in a Hydrogel Model of Vocal Fold Lamina Propria. Regenerative Engineering and Translational Medicine. 2018. doi:10.1007/s40883-018-0085-8.
17. Tong Z, Duncan RL, Jia X. Modulating the behaviors of mesenchymal stem cells via the combination of high-frequency vibratory stimulations and fibrous scaffolds. Tissue engineering Part A. 2013;19(15-16):1862-78. doi:10.1089/ten.TEA.2012.0694.
18. Sapozhnikov OA, Morozov AV, Cathignol D, editors. Piezoelectric transducer surface vibration characterization using acoustic holography and laser vibrometry. IEEE Ultrasonics Symposium, 2004; 2004 23-27 Aug. 2004.
19. Holzapfel GA. Nonlinear Solid Mechanics: A Continuum Approach for Engineering Science. vol 4. Wiley; 2002.
20. ANSYS® Academic Research Mechanical. Help System, Coupled Field Analysis Guide: ANSYS, Inc.
21. Papadopoulou A, Iliadi A, Eliades T, Kletsas D. Early responses of human periodontal ligament fibroblasts to cyclic and static mechanical stretching. Eur J Orthod. 2017;39(3):258-63. doi:10.1093/ejo/cjw075.
22. Angel P, Karin M. The role of Jun, Fos and the AP-1 complex in cell-proliferation and transformation. Biochim Biophys Acta. 1991;1072(2-3):129-57.
23. Karin M. The regulation of AP-1 activity by mitogen-activated protein kinases. J Biol Chem. 1995;270(28):16483-6.
24. Karin M, Liu Z, Zandi E. AP-1 function and regulation. Curr Opin Cell Biol. 1997;9(2):240-6.
25. Hinz B, Phan SH, Thannickal VJ, Galli A, Bochaton-Piallat ML, Gabbiani G. The myofibroblast: one function, multiple origins. Am J Pathol. 2007;170(6):1807-16. doi:10.2353/ajpath.2007.070112.
26. Tong X, Yang F. Sliding Hydrogels with Mobile Molecular Ligands and Crosslinks as 3D Stem Cell Niche. Adv Mater. 2016;28(33):7257-63. doi:10.1002/adma.201601484.
27. Castillo Diaz LA, Elsawy M, Saiani A, Gough JE, Miller AF. Osteogenic differentiation of human mesenchymal stem cells promotes mineralization within a biodegradable peptide hydrogel. J Tissue Eng. 2016;7:2041731416649789. doi:10.1177/2041731416649789.
28. Goding J, Gilmour A, Robles UA, Poole-Warren L, Lovell N, Martens P et al. A living electrode construct for incorporation of cells into bionic devices. MRS Communications. 2017;7(3):487-95. doi:10.1557/mrc.2017.44.
29. Farran AJ, Teller SS, Jia F, Clifton RJ, Duncan RL, Jia X. Design and characterization of a dynamic vibrational culture system. J Tissue Eng Regen Med. 2013;7(3):213-25. doi:10.1002/term.514.
30. Zhang K, Siegmund T, Chan RW. Modeling of the transient responses of the vocal fold lamina propria. J Mech Behav Biomed Mater. 2009;2(1):93-104. doi:10.1016/j.jmbbm.2008.05.005.

31. Chan A, Mongeau L, Kost K. Vocal fold vibration measurements using laser Doppler vibrometry. J Acoust Soc Am. 2013;133(3):1667-76. doi:10.1121/1.4789937.
32. Kutty JK, Webb K. Vibration stimulates vocal mucosa-like matrix expression by hydrogel-encapsulated fibroblasts. J Tissue Eng Regen Med. 2010;4(1):62-72. doi:10.1002/term.219.
33. Titze IR, Hitchcock RW, Broadhead K, Webb K, Li W, Gray SD et al. Design and validation of a bioreactor for engineering vocal fold tissues under combined tensile and vibrational stresses. J Biomech. 2004;37(10):1521-9. doi:10.1016/j.jbiomech.2004.01.007.
34. Wernig F, Mayr M, Xu Q. Mechanical stretch-induced apoptosis in smooth muscle cells is mediated by beta1-integrin signaling pathways. Hypertension. 2003;41(4):903-11. doi:10.1161/01.HYP.0000062882.42265.88.
35. Dicker KT, Gurski LA, Pradhan-Bhatt S, Witt RL, Farach-Carson MC, Jia X. Hyaluronan: a simple polysaccharide with diverse biological functions. Acta Biomater. 2014;10(4):1558-70. doi:10.1016/j.actbio.2013.12.019.
36. Caskey RC, Allukian M, Lind RC, Herdrich BJ, Xu J, Radu A et al. Lentiviral-mediated over-expression of hyaluronan synthase-1 (HAS-1) decreases the cellular inflammatory response and results in regenerative wound repair. Cell Tissue Res. 2013;351(1):117-25. doi:10.1007/s00441-012-1504-7.
37. Larson BJ, Longaker MT, Lorenz HP. Scarless fetal wound healing: a basic science review. Plastic and reconstructive surgery. 2010;126(4):1172-80. doi:10.1097/PRS.0b013e3181eae781.
38. Leavitt T, Hu MS, Marshall CD, Barnes LA, Lorenz HP, Longaker MT. Scarless wound healing: finding the right cells and signals. Cell Tissue Res. 2016;365(3):483-93. doi:10.1007/s00441-016-2424-8.
39. Wang CJ. Extracorporeal shockwave therapy in musculoskeletal disorders. J Orthop Surg Res. 2012;7:11. doi:10.1186/1749-799X-7-11.
40. Zhou S, Bachem MG, Seufferlein T, Li Y, Gross HJ, Schmelz A. Low intensity pulsed ultrasound accelerates macrophage phagocytosis by a pathway that requires actin polymerization, Rho, and Src/MAPKs activity. Cell Signal. 2008;20(4):695-704. doi:10.1016/j.cellsig.2007.12.005.
41. Young SR, Dyson M. Macrophage responsiveness to therapeutic ultrasound. Ultrasound Med Biol. 1990;16(8):809-16.
42. Kirsch A, Hortobagyi D, Stachl T, Karbiener M, Grossmann T, Gerstenberger C et al. Development and validation of a novel phonomimetic bioreactor. PLoS One. 2019;14(3):e0213788. doi:10.1371/journal.pone.0213788.
43. Russell KC, Phinney DG, Lacey MR, Barrilleaux BL, Meyertholen KE, O'Connor KC. In vitro high-capacity assay to quantify the clonal heterogeneity in trilineage potential of mesenchymal stem cells reveals a complex hierarchy of lineage commitment. Stem Cells. 2010;28(4):788-98. doi:10.1002/stem.312.
44. Lv FJ, Tuan RS, Cheung KM, Leung VY. Concise review: the surface markers and identity of human mesenchymal stem cells. Stem Cells. 2014;32(6):1408-19. doi:10.1002/stem.1681.
45. Steingen C, Brenig F, Baumgartner L, Schmidt J, Schmidt A, Bloch W. Characterization of key mechanisms in transmigration and invasion of mesenchymal stem cells. J Mol Cell Cardiol. 2008;44(6):1072-84. doi:10.1016/j.yjmcc.2008.03.010.
46. Mabuchi Y, Morikawa S, Harada S, Niibe K, Suzuki S, Renault-Mihara F et al. LNGFR(+)THY-1(+)VCAM-1(hi+) cells reveal functionally distinct subpopulations in

mesenchymal stem cells. Stem Cell Reports. 2013;1(2):152-65. doi:10.1016/j.stemcr.2013.06.001.
47. Hossain MG, Iwata T Fau - Mizusawa N, Mizusawa N Fau - Shima SWN, Shima Sw Fau - Okutsu T, Okutsu T Fau - Ishimoto K, Ishimoto K Fau - Yoshimoto K et al. Compressive force inhibits adipogenesis through COX-2-mediated down-regulation of PPARgamma2 and C/EBPalpha. (1347-4421 (Electronic)).
48. Petkova DK, Clelland CA, Ronan JE, Lewis S, Knox AJ. Reduced expression of cyclooxygenase (COX) in idiopathic pulmonary fibrosis and sarcoidosis. Histopathology. 2003;43(4):381-6.
49. Davids JS, Carothers AM, Damas BC, Bertagnolli MM. Chronic cyclooxygenase-2 inhibition promotes myofibroblast-associated intestinal fibrosis. Cancer Prev Res (Phila). 2010;3(3):348-58. doi:10.1158/1940-6207.CAPR-09-0146.
50. Branski RC, Perera P, Verdolini K, Rosen CA, Hebda PA, Agarwal S. Dynamic biomechanical strain inhibits IL-1beta-induced inflammation in vocal fold fibroblasts. J Voice. 2007;21(6):651-60. doi:10.1016/j.jvoice.2006.06.005.
51. Giannandrea M, Parks WC. Diverse functions of matrix metalloproteinases during fibrosis. Dis Model Mech. 2014; 7(2):193-203. doi: 10.1242/dmm.012062.
52. Gaffney J, Solomonov I, Zehorai, E, Sagi I. Multilevel regulation of matrix metalloproteinases in tissue homeostasis indicates their molecular specificity in vivo. Matrix Biol, 2015; 44-46:191-0. doi: 10.1016/j.matbio.2015.01.012.

Gene	Forward Primer (5'-3')	Reverse Primer (5'-3')	GeneBank Number	Efficiency	Product Size (bp)
FN	ACCTACGGATGACT CGTGCTTTGA	CAAAGCCTAAGCAC TGGCACAACA	NM_001306132	2.10	116
MMP2	GCCAATGGAGACT GTCTCAAGA	TTCTAAGGCAGCCA GCAGTGAA	NM_001302510	1.87	122
COL1α1	AATGGTGCTCCTG GTATTGCTGGT	ACCAGTGTCTCCTT TGCTGCCA	XM_005257058	2.10	141
CTGF	AGGAGTGGGTGTG TGACGA	CCAGGCAGTTGGCT CTAATC	NM_001901	1.90	117
FNEDA	CCCTAAAGGACTG GCATTCA	CATCCTCAGGGCTC GAGTAG	XM_017003692	1.99	113
VCAM	AGTTGAAGGATGC GGGAGTAT	GGATGCAAAATAGA GCACGAG	NM_001078	1.99	143
COX2	GCCCAGCACTTCA CGCATCAG	AGACCAGGCACCAG ACCAAAGACC	NM_000963	1.92	290
C-Fos	CTACCACTCACCC GCAGACT	AGGTCCGTGCAGAA GTCCT	NM_005252	1.97	72
LOX	GCGCTGTGACATTC GCTACA	GCTTTGCCTTCTAAT ACGGTGAA	NM_002317	2.00	77

Table 1. Oligonucleotide primer sequences, accession numbers, efficiencies, and product sizes. Gene abbreviations: GAPDH, glyceraldehyde-3-phosphate dehydrogenase; FN, fibronectin; MMP1, matrix metalloproteinase 1; MMP2, matrix metalloproteinase 2; COL3α1, collagen type III alpha-1 chain; COL1α1, collagen type I alpha-1 chain; HAS1, hyaluronic acid synthase 1; CTGF, connective tissue growth factor; αSMA, alpha-smooth muscle actin; FNEDA, fibronectin extra domain-A; MCAM, melanoma cell adhesion molecule; VCAM, vascular cell adhesion molecule; p53, tumor protein p53; COX2, cyclooxygenase 2; c-Jun, jun proto-oncogene; c-Fos, fos proto-oncogene; EGR-1, early growth response 1; LOX, lysyl oxidase.

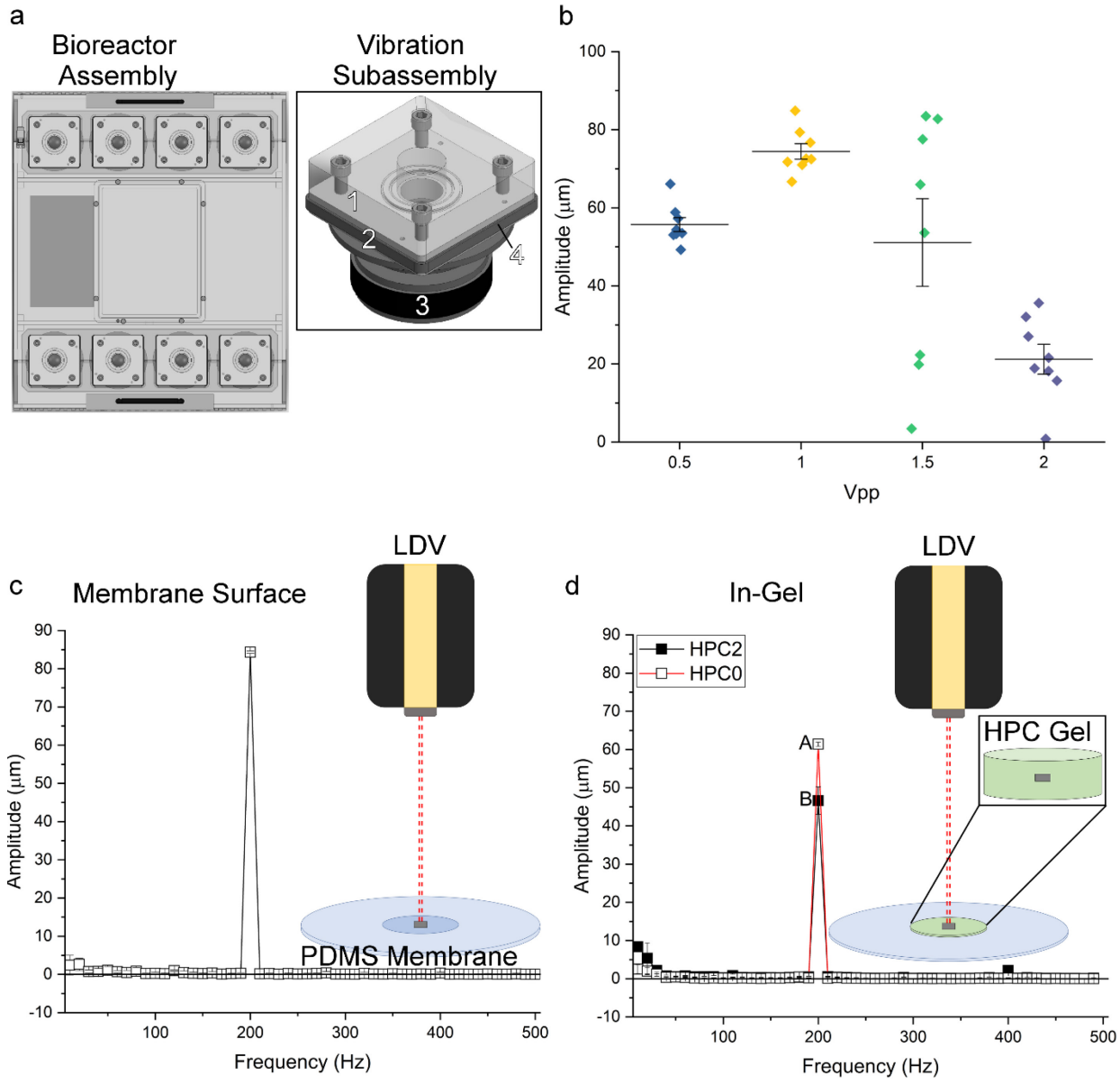

Figure 1. Vibrational amplitude characterization by LDV. (A) Schematic of bioreactor assembly (top view) and individual vibration subassembly (isometric view). (1) Upper block, (2) lower block, (3) speaker, and (4) silicone vibrational isolators. (B) Quantification of PDMS membrane vibrational centerpoint amplitude at 200 Hz while varying peak-to-peak voltage (V_{pp}). (C) Fast Fourier transform (FFT) distribution of PDMS membrane surface vibrational center point amplitude at 200 Hz driving frequency. (D) FFT distribution of vibrational centerpoint amplitude within HPC2 and HPC0 hydrogel formulations. Different letters indicate significant difference compared to HPC0 controls ($p<0.05$).

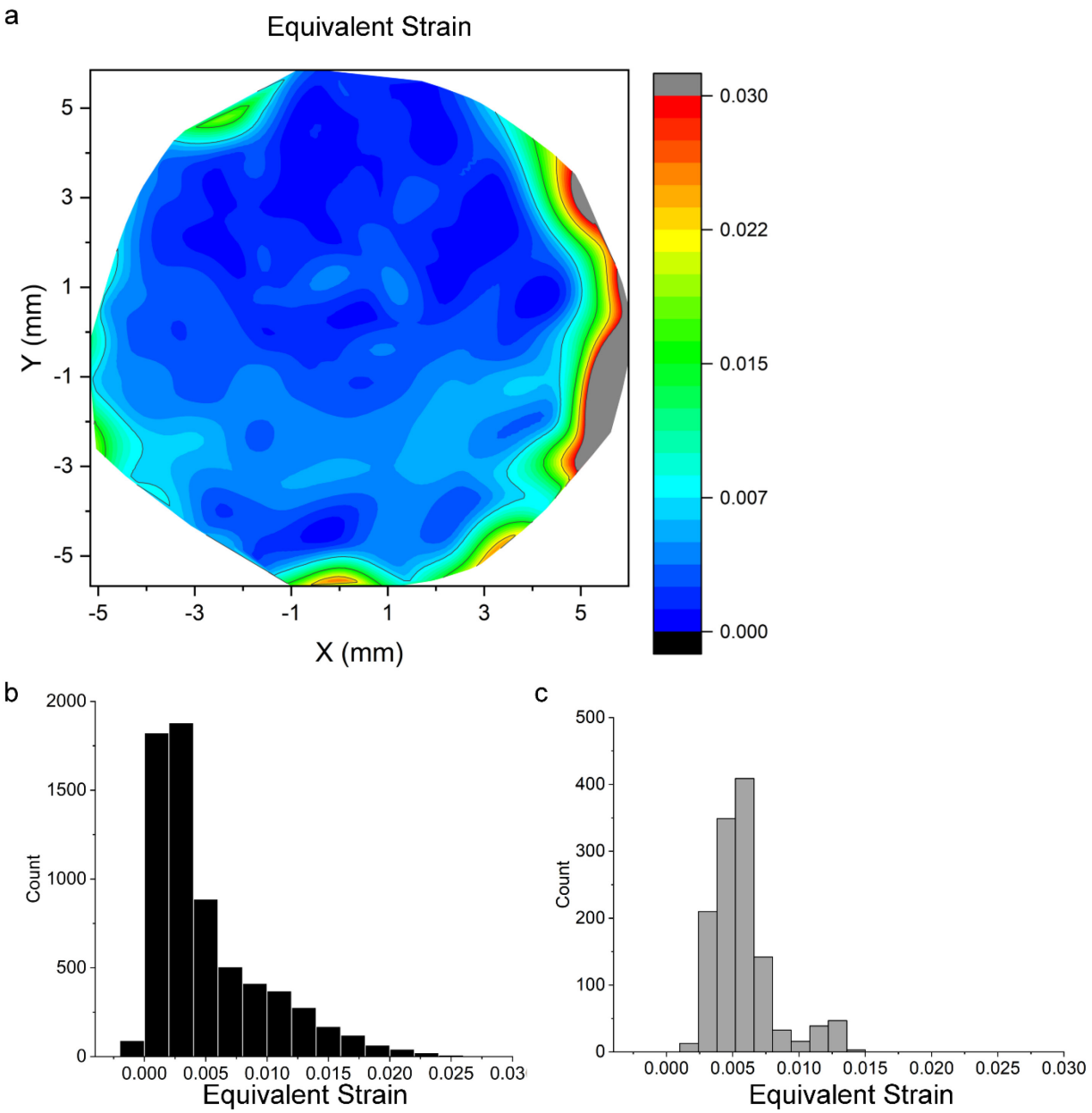

Figure 2. Bioreactor characterization by DIC. (A) Representative contour plot of equivalent strain (ε_{xy}) across the PDMS membrane central envelope as determined by DIC at the moment of highest oscillatory amplitude. (B) Histogram of equivalent strain across the PDMS membrane surface (red circle) as determined by 2D DIC. (C) Histogram of predicted equivalent strain across the PDMS surface as determined by FEA.

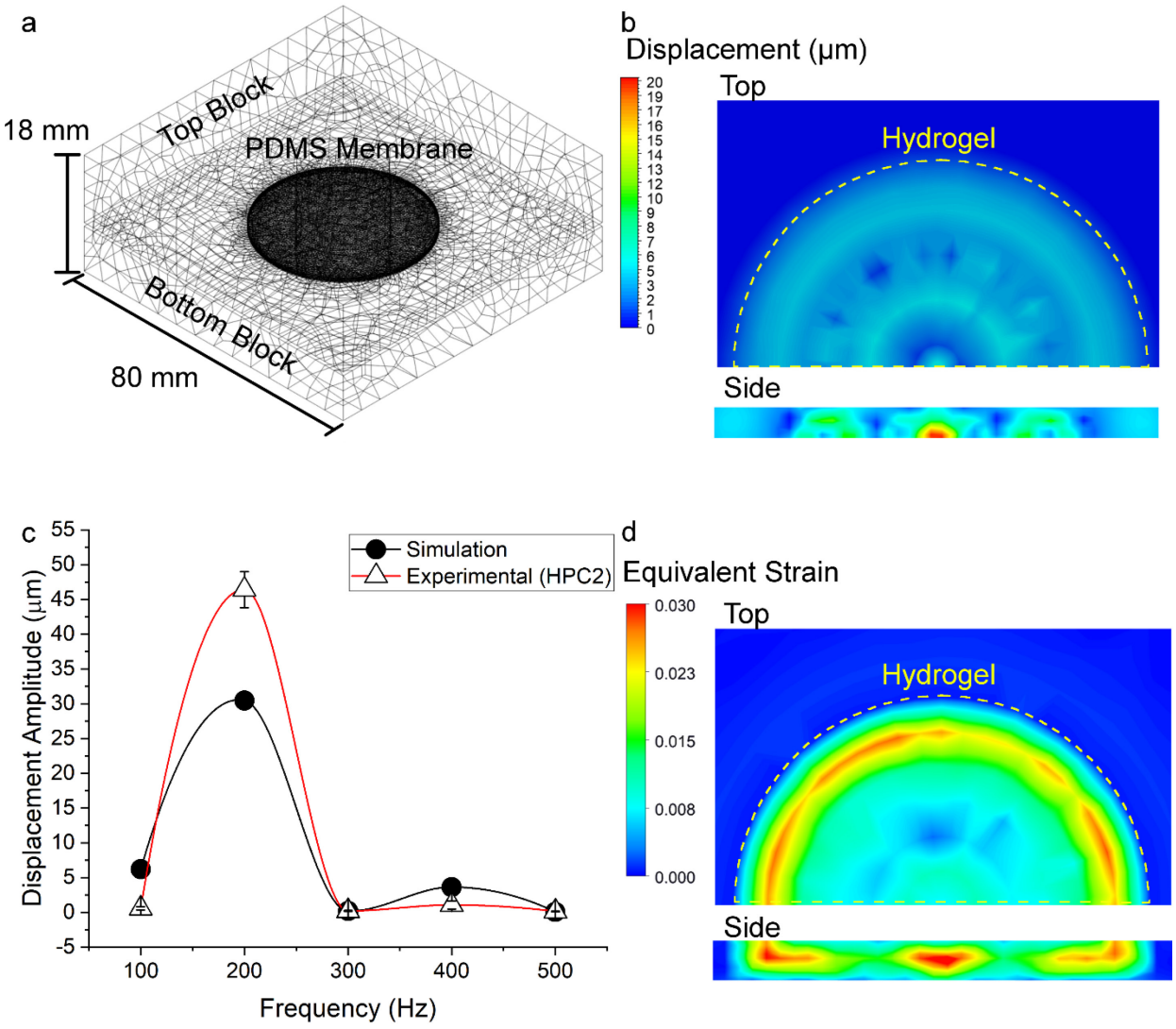

Figure 3. Development, validation, and implementation of FEA model of in-gel strain. (A) Visualization of vibrational assembly geometry and computational model domains shown as an isometric view. (B) Visualization of predicted hydrogel displacement over the hydrogel surface and within a cross-sectional area of the hydrogel component. (C) Comparison between predicted in-gel vibrational amplitude and LDV experimental values. The experimental and the simulation results overlap for 300 and 500 Hz. (D) Visualization of predicted strain distribution across the hydrogel surface and within a cross-sectional area of the hydrogel component.

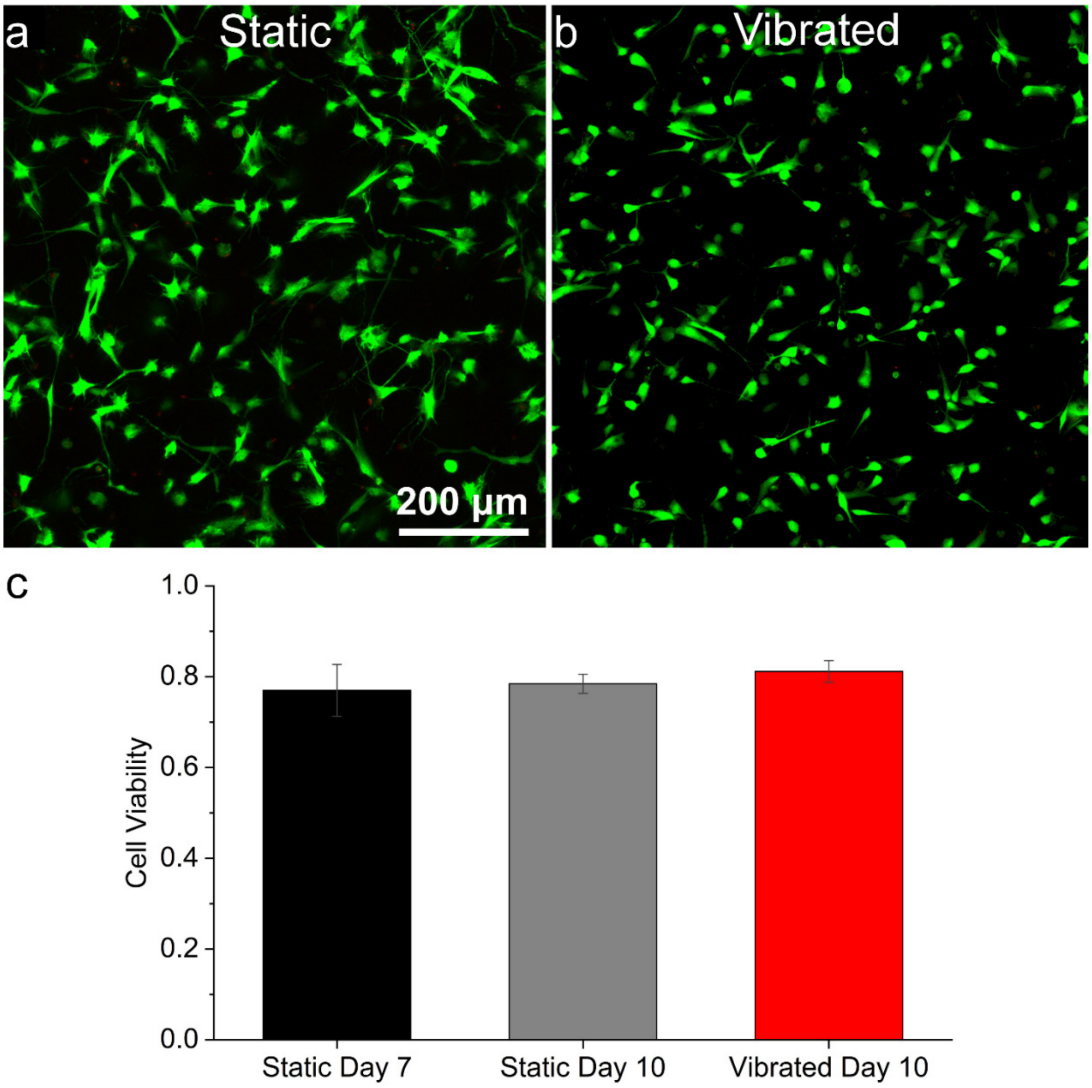

Figure 4. Cell viability in HPC2 Hydrogels following vibration. (A-B) LIVE/DEAD staining on gels at day 10 in (A) static controls or (B) gels vibrated for 3 days. Live cells were stained green and dead cells were stained red by calcein AM and ethidium homodimer, respectively. Magnification: 10 ×. Scale bar: 200 µm. (C) Quantified percent viable cells compared to day 7 samples before vibration.

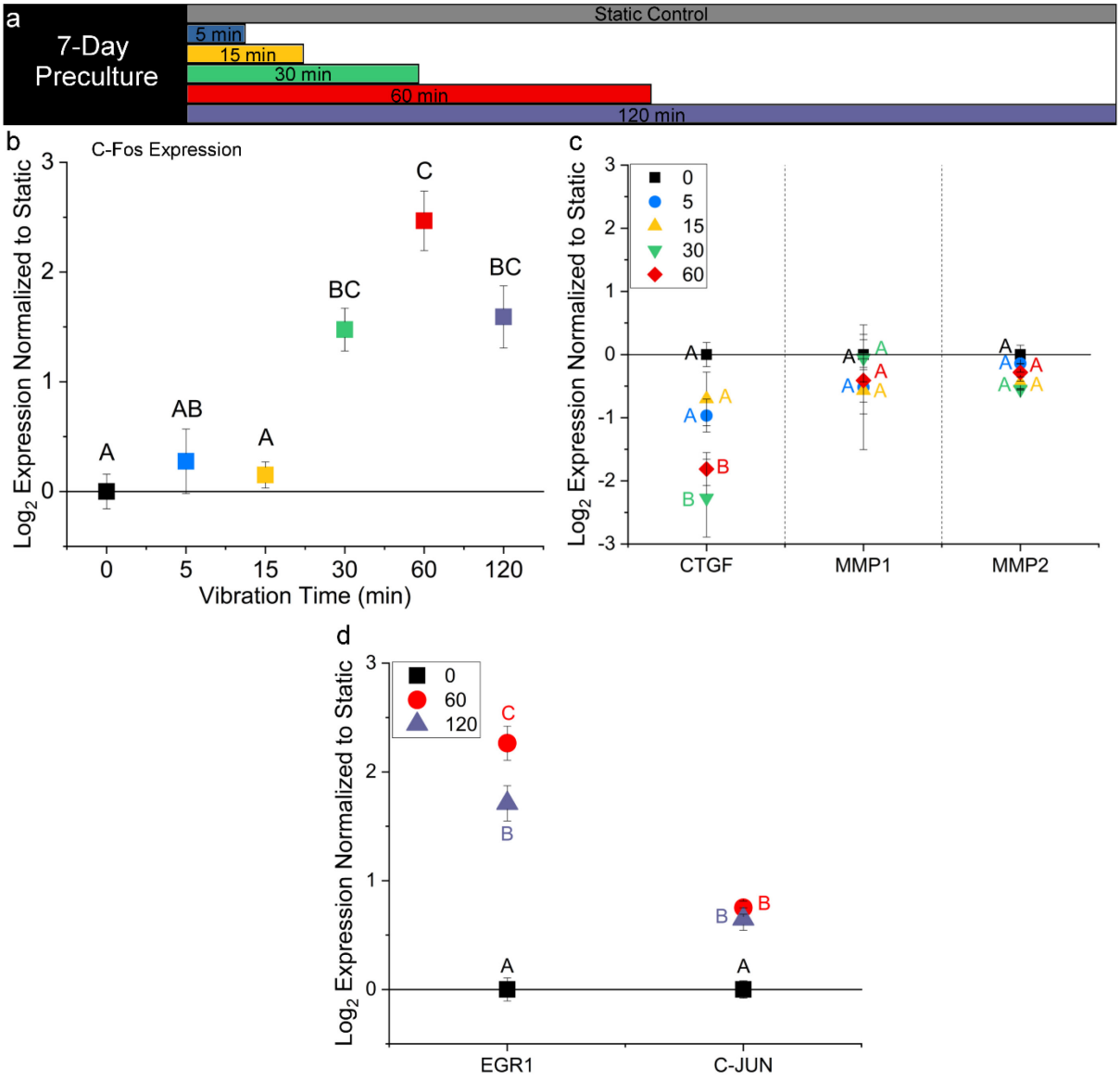

Figure 5. Time-dependent gene expression of hMSCs cultured in HPC gels in the presence of vibrational stimulation. (A) Experimental design for the time course study. (B) c-Fos expression as a function of vibration durations. (C) Time-dependent expression of CTGF, MMP1 and MMP2. (D) Time-dependent expression of additional immediate-early genes. Different letters indicate significant difference compared to static controls ($p<0.05$).

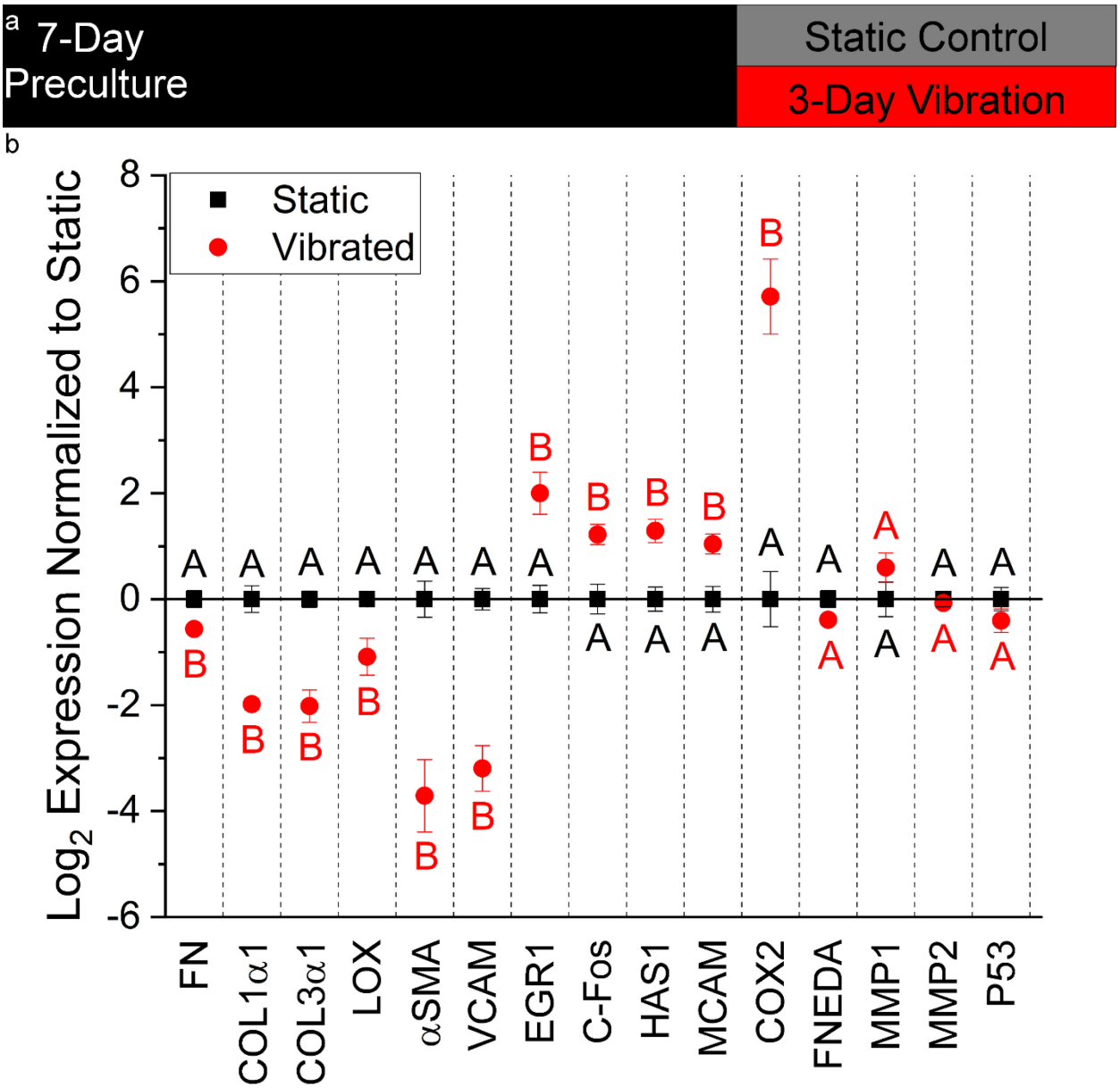

Figure 6. Changes in gene expression following 3-day vibratory period. (A) Timecourse of vibrational culture. (B) Gene expression in HPC2 cell/gel constructs after 3-day vibration at 200 Hz on a 1h-on 1h-off cycle. Different letters indicate significant difference compared to static controls ($p<0.05$).

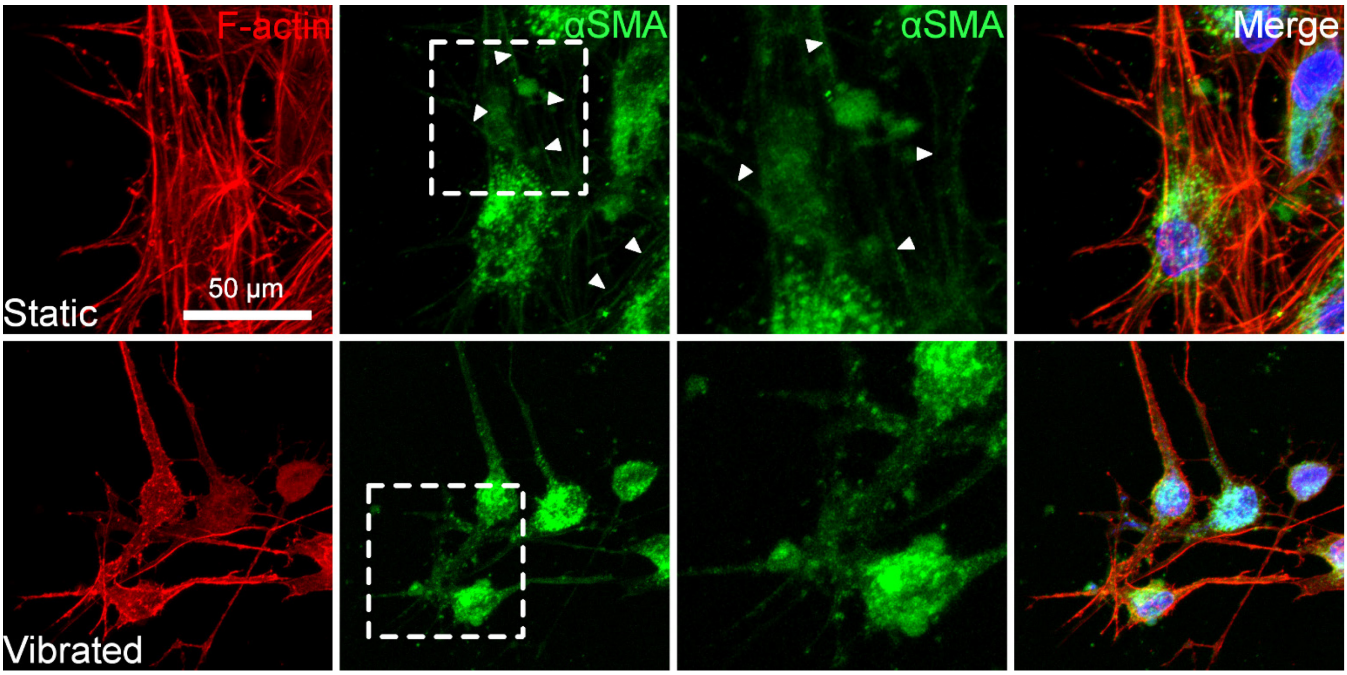

Figure 7. Immunofluorescence imaging of αSMA expression in HPC2 hydrogels following 3-day vibration. White arrows indicate the presence of αSMA overlapping F-actin stress fibers. White dashed box indicates area of magnification in following image αSMA image. Samples were stained with DAPI (blue), anti-αSMA (green), and phalloidin (red). Magnification: 25×. Scale: 50 μm.